Thermal Stability and Thermodynamics of the Ag_2ZnGeS_4 Compound

Mykola Moroz,✉ Fiseha Tesfaye, Pavlo Demchenko, Myroslava Prokhorenko, Daniel Lindberg, Oleksandr Reshetnyak, Leena Hupa

Abstract

Phase equilibria in the ZnS–Ag_2GeS_3–Ge–GeS_2 part of the Ag–Zn–Ge–S system were investigated using differential thermal analysis, X-ray diffraction, and EMF methods. The data was used to model Ag_2GeS_3–ZnS polythermal section. Further, the mechanism of formation and thermal stability of the Ag_2ZnGeS_4 compound were established. The results suggest presence of another quaternary phase $Ag_4ZnGe_2S_7$ ~~exists~~ in the temperature range of 695 to 853 K. The determined phase relations were used to express the chemical reactions. Based on the electromotive force vs. temperature measurements, experimental thermodynamic data of the Ag_2ZnGeS_4 quaternary phase were derived for the first time. The calculated Gibbs energy, enthalpy and entropy values of the Ag_2ZnGeS_4 compound in both phase regions are consistent, which indicates that Ag_2ZnGeS_4 has stoichiometric composition.

Keywords Chalcogenide semiconductors, Phase equilibria, Thermodynamic properties, EMF method, Gibbs energy

1. Introduction

The stannite-type quaternary compounds of the general composition Ag_2BCX_4 (B = Zn, Cd, Hg, Pb, Fe, Mn; C = Si, Ge, Sn; X = S, Se, Te) exist in the Ag–B–C–X systems [1,2]. These compounds crystallize in tetrahedral structures of the mineral stannite or in the ordered wurtzite structure [1,3]. These crystallographic forms are close to each other with the only difference in the distribution of the cations in the tetrahedral sites [4]. Each metal cation is tetrahedrally coordinated by four sulfur anions [1]. The stannite-type compounds have been studied as materials for low-cost solar cells, high-efficiency light emitting diodes [1,4–6], and thermoelectric applications [7]. In addition, the Ag_2BCX_4 semiconducting compounds are promising materials for photocatalytic hydrogen production [8]. Some of these compounds have acentric crystalline structure and can be used as materials in non-linear optics, spin- and optoelectronics applications [9]. Such interesting applications are stimulating further research efforts towards to expand the areas of use of these semiconductors.

Four-element compounds with B = Zn, Cd, Hg and X = S are located in the Ag_2X–BX–CX_2 (I) systems [2,10,11]. In the Ag_2S–ZnS–GeS_2 (II) system only one quaternary compound Ag_2ZnGeS_4 (III) is found [2]. It crystallizes in the tetragonal structure (space group $I\bar{4}2m$, a = 0.574996(9) nm, c = 1.03434(3) nm, c/a = 1.799). The phase equilibria at $T \leq 670$ K and glass formation region of the Ag_2S–GeS_2–ZnS system have

M. Moroz, F. Tesfaye, L. Hupa
Laboratory of Inorganic Chemistry, Johan Gadolin Process Chemistry Centre, Åbo Akademi University, 20500 Turku, Finland

P. Demchenko
Department of Inorganic Chemistry, Ivan Franko National University of Lviv, 79005 Lviv, Ukraine

M. Prokhorenko
Department of Cartography and Geospatial Modeling, Lviv Polytechnic National University, 79013 Lviv, Ukraine

D. Lindberg
School of Chemical Engineering, Aalto University, 02150 Espoo, Finland

O. Reshetnyak
Department of Physical and Colloid Chemistry, Ivan Franko National University of Lviv, 79005 Lviv, Ukraine

✉ Corresponding author. E-mail address: riv018@i.ua

been investigated by Parasyuk et al. [2]. The energy gap of the Ag_2ZnGeS_4 compound is equal to 2.5 eV [1]. The phase equilibria (II) are represented by the cross-sections that connect (III) with binary compounds (II), ternary compounds Ag_8GeS_6, $Ag_{10}Ge_3S_{11}$, Ag_2GeS_3, and the Ag_8GeS_8–ZnS tie line. The phase diagram of the Ag_8GeS_8–ZnS system was investigated by Piskach et al. [12]. It is of the eutectic type, with the invariant point at T = 1201 K and 42 mol.% ZnS. The solubility of ZnS in Ag_8GeS_6 at T = 499 K is ~15 mol.% ZnS [2]. The mechanism of formation and the thermal stability of the Ag_2ZnGeS_4 compound have not been established.

Two quaternary compounds Ag_2CdGeS_4 and $Ag_4CdGe_2S_7$ exist in the Ag_2S–CdS–GeS_2 system [10]. Four-element phase region of the Ag_2S–HgS–GeS_2 system is characterized by the presence of the ~$Ag_4HgGe_2S_7$, Ag_2HgGeS_4, $Ag_2Hg_3GeS_6$, and $Ag_6Hg_{0.82}GeS_{5.82}$ compounds [11]. The homogeneity range of the $Ag_6Hg_{0.82}GeS_{5.82}$ phase along the Ag_8GeS_6–Hg_4GeS_6 section at T = 670 K is equavalent to 22 to 31 mol.% Hg_4GeS_6.

The presence of a wide glass formation region nearAg_2S–GeS_2 system causes the appearance of kinetic obstacles to the equilibrium crystallization of phases from melts, the polymorphic phase transitions, and change of the regions of stabilities of some phases [2]. In this case, the choice of optimal conditions for the synthesis of compounds to achieve thermodynamic equilibrium is more complicated. These experimental difficulties in the study of phase relations in (I) can partially be solved through theoretical calculations of the T–x phase diagrams using, for example, the CALPHAD methods [13,14]. These methods are based on thermodynamic data of the pure phases together with experimentally constructed T–x diagrams of separate sections.

In this work, we present the results of the phase equilibria in the vicinity of Ag_2ZnGeS_4 compound of the Ag–Zn–Ge–S system. Furthermore, we determined the thermodynamic properties of the quaternary phase in this system quantitatively.

2. Experimental Section

2.1 Synthesis

The starting materials for synthesis were high-purity elements (99.99 wt.% Ag, 99.999 wt.% Ge, 99.99 wt.% S, and 99.99 wt.% ZnS). The synthesis and annealing were performed in thin-walled evacuated quartz glass ampoules with a residual pressure ≤ 1 Pa. Compounds GeS, GeS_2, and Ag_2GeS_3 were synthesized by cooling appropriately mixed melts of elements from T = 1170 K. Compounds Ag_2ZnGeS_4 and $Ag_4ZnGe_2S_7$ were obtained through solid-state synthesis from finely dispersed mixtures of Ag_2GeS_3 and ZnS at T = 750 K for 300 h. Differential thermal analysis (DTA) and X-ray diffraction (XRD) methods were used to characterize the composition of the synthesized compounds. The Ag_2GeS_3 glass [15,16] was obtained by melt quenching of the corresponding elements from T = 1200 K in ice water.

2.2 Thermal Analysis Methods

DTA curves of the samples were recorded using a Paulik-Paulik-Erdey derivatograph fitted with chromel-alumel thermocouples and an H307-1 XY recorder. The heating and cooling rates in the DTA measurements of the samples were in the range of 6 to 8 K·min^{-1} [17]. The thermocouples were calibrated by the melting temperatures of In (T = 429 K), Sn (T = 505 K), Cd (T = 594 K), Te (T = 723 K), Sb (T = 904 K), NaCl (T = 1074 K), Ge (T = 1209 K), Ag (T = 1236 K), and Cu (T = 1357 K) [18]. Errors in the temperature measurements were below ΔT = ± 3 K.

Differential scanning calorimetry (DSC) and thermogravimetric (TG) analysis of the compounds were done by using a NETZSCH STA 449 F1 Jupiter® equipment. The calorimeter was calibrated with the melting temperatures and enthalpies of fusion for high purity chemical elements Sn, In, Bi, Zn, Al, and Au [18]. The average measurement accuracies of temperatures and enthalpies of fusion were determined to be ΔT = ± 1 K and ΔH = ± 1.14%, respectively. To remove traces of reactive gases such as O_2(g), the chamber was evacuated and then backfilled with pure Ar(g) three times before each run. The purging gas Ar(g) at pressure 1×10^5 Pa was also used as a protective gas. The flow rate of the protective Ar(g) was 50 ml min^{-1} in all runs. The heating and cooling rates in the DSC-TG measurements of the samples were 10 K min^{-1}.

XRD patterns were collected on a STOE STADI P diffractometer equipped with a linear position–sensitive detector PSD, in a modified Guinier geometry (transmission mode, Cu$K\alpha_1$ radiation, a bent Ge (111) monochromator, $2\theta/\omega$ scan mode). Preliminary data processing and X-ray phase analyses were performed using STOE WinXPOW 3.03 [19] and PowderCell 2.4 PC programs [20], using data on crystal structures for the phases taken from database [21].

2.3 Electromotive Force Measurements

For electromotive force (EMF) measurements [22,23], the following electrochemical cells (ECCs) were assembled:

(–) C | Ag | Ag_2GeS_3 glass | Ag_2ZnGeS_4, GeS, GeS_2, ZnS | C (+) (i)

(–) C | Ag | Ag_2GeS_3 glass | Ag_2ZnGeS_4, GeS, Ge, ZnS | C (+) (ii)

where C is graphite and Ag_2GeS_3 glass is the fast purely Ag^+ ions conducting electrolyte [15]. Ag_2GeS_3 glass has similar ionic properties with superionic materials Ag_3GeS_3I and Ag_3GeS_3Br [24,25]. The vertical lines in ECCs (i) and (ii) indicate phase boundaries or contacts between cell components. Commas between compounds mean mechanical mixtures of the phases. The cell polarities and half-cell reactions in the ECCs were established according to rules described in [22,26].

As positive (right) electrodes of the ECCs, we used the equilibrium samples. The positive electrodes in the ECCs (i) and (ii) were prepared by solid state synthesis of (Ag_2ZnGeS_4 : GeS : GeS_2 : ZnS) in the molar ratio 1 : 1 : 2 : 1 and (Ag_2ZnGeS_4 : GeS : Ge : ZnS) in the molar ratio 1 : 3 : 2 : 1, respectively. The equilibrium state of four-phases sample was achieved by vacuum annealing at 750 K for 240 h. Components of the ECCs in powder form were pressed at 10^8 Pa through a 2 mm diameter hole arranged in the fluoroplast matrix up to density $\rho = (0.93 \pm 0.02)\cdot\rho_0$, where ρ_0 is the experimentally determined density of cast samples. Five-fold thermal cycling of ECCs in the range of 400 to 550 K was performed to eliminate possible defects due to plastic deformation during sample pressing. The heating and cooling rates were of 2 K min^{-1}. Experiments were performed in a horizontal resistance furnace, similar to that described in [27]. As protective atmosphere, we used a continuously flowing highly purified (0.9999 volume fraction) Ar(g) at $P = 1.2\cdot10^5$ Pa, with a flow rate of $2\cdot10^{-3}$ m^3 h^{-1} from the right to left electrode of the ECCs. The temperature was maintained with an accuracy of ± 0.5 K. The EMF of the cells were measured by high-resistance (input impedance of $>10^{12}$ Ω) universal U7-9 digital voltmeter. The equilibrium in ECCs at each temperature was achieved within 2 h. After equilibrium has been attained, the EMF values were constant or their variation did not exceed ± 0.2 mV. The dependences of the EMF of the cells on temperature $E(T)$ were analyzed by the method described in [23].

3. Results and Discussion

3.1 Phase Equilibria

Phase equilibria in the ZnS–Ag_2GeS_3–Ge–GeS_2 (IV) part of the Ag–Zn–Ge–S system are shown in Fig. 1.

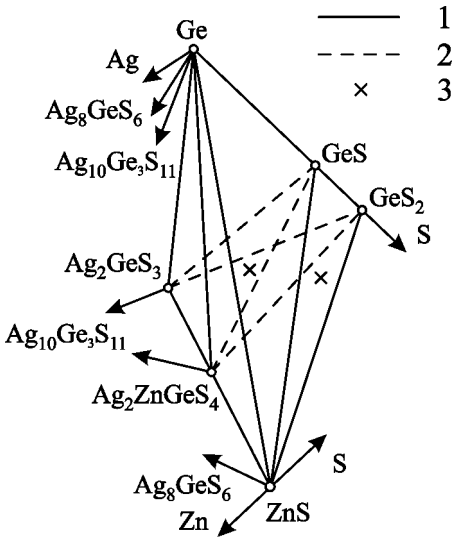

Fig. 1 The phase equilibria of the Ag–Zn–Ge–S system in the ZnS–Ag_2GeS_3–Ge–GeS_2 part, below T = 650 K. 1 and 2 are the lines of two-phase equilibria, 3 is compositions of positive electrodes of ECCs

The presence of four subsystems have been established: Ag_2GeS_3–Ge–GeS–Ag_2ZnGeS_4, Ag_2GeS_3–GeS_2–GeS–Ag_2ZnGeS_4, Ag_2ZnGeS_4–GeS–GeS_2–ZnS (V), and Ag_2ZnGeS_4–GeS–Ge–ZnS (VI). Some studies concerning the phase composition of compounds (IV) have been reported earlier in [2]. Our experimental results are presented in Figs. 2-4.

Two-phase state of the Ag_2ZnGeS_4–Ge section without the formation of intermediate phases is confirmed by the diffraction patterns presented in Fig. 2. The diffraction peaks of the Ag_2ZnGeS_4 and Ge matching with JCPDS cards no. 00-059-0249 and 00-0040545, respectively [21]. According to obtained XRD results, the Ag_2ZnGeS_4 crystallized in the structure type of Cu_2FeSnS_4 compound (space group $I\bar{4}2m$, a = 0.57459(7) nm, c = 1.0332(1) nm, V = 0.34198 nm^3). The obtained crystallographic data for Ag_2ZnGeS_4 compound are in good agreement with the results reported by Parasyuk et al. [2]. Two-phase state of the ZnS–GeS and Ag_2ZnGeS_4–GeS cross-sections at T<600 K have been established by the EMF method [22,23]. The EMF values of the galvanic cells with the positive electrodes from the phase regions (V) and (VI) at T = const do not depend on molar ratio of phases.

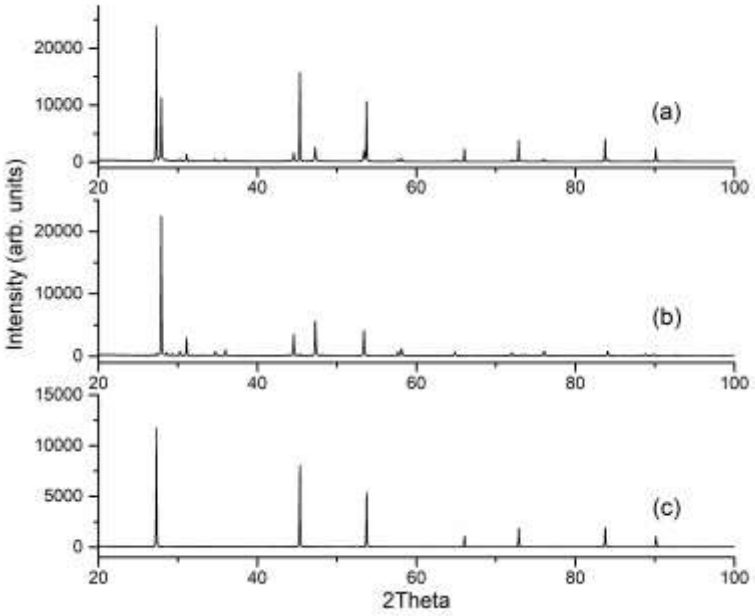

Fig. 2 XRD patterns for different compositions in the Ag_2ZnGeS_4–Ge system: (a) 50 mol.% Ag_2ZnGeS_4 – 50 mol.% Ge, (b) Ag_2ZnGeS_4, (c) Ge

The phase diagram of the Ag_2GeS_3–ZnS system is shown in Fig. 3. Some boundary lines in the concentration range of 65 to 100 mol.% Ag_2GeS_3 are marked by dashed lines due to a large viscosity of the melts.

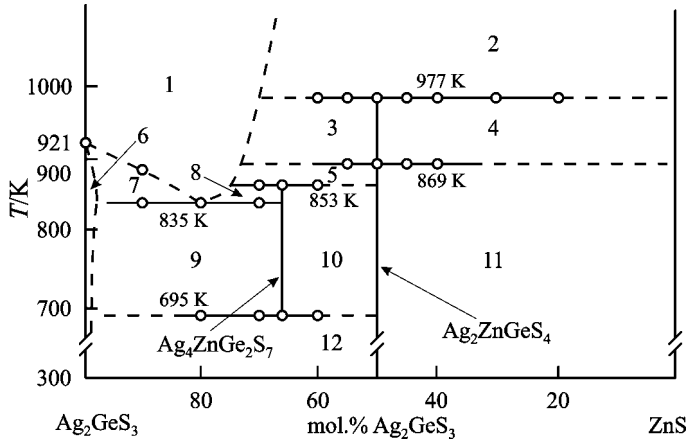

Fig. 3 Phase diagram of the Ag_2GeS_3–ZnS system. (1) L, (2) L + ZnS, (3) L + α-Ag_2ZnGeS_4, (4) α-Ag_2ZnGeS_4 + ZnS, (5) L + β-Ag_2ZnGeS_4, (6) α-Ag_2GeS_3, (7) L + α-Ag_2GeS_3, (8) L + $Ag_4ZnGe_2S_7$, (9) α-Ag_2GeS_3 + $Ag_4ZnGe_2S_7$, (10) $Ag_4ZnGe_2S_7$ + β-Ag_2ZnGeS_4, (11) β-Ag_2ZnGeS_4 + ZnS, (12) α-Ag_2GeS_3 + β-Ag_2ZnGeS_4

This phase diagram is of the eutectic type with the formation of the Ag_2ZnGeS_4 and $Ag_4ZnGe_2S_7$ quaternary compounds. The eutectic point lies at 833 K and 20 mol.% ZnS. According to our experimental results, the

Ag_2ZnGeS_4 compound is formed at 977 K in a peritectic reaction L + ZnS → Ag_2ZnGeS_4 and shows the phase transition at 869 K. The $Ag_4ZnGe_2S_7$ intermediate compound is formed by the peritectic reaction L + Ag_2ZnGeS_4 → $Ag_4ZnGe_2S_7$ at 853 K and decomposes below 695 K to Ag_2ZnGeS_4 and Ag_2GeS_3.

The results of DSC-TG measurement of the Ag_2ZnGeS_4 compound is presented in Fig. 4.

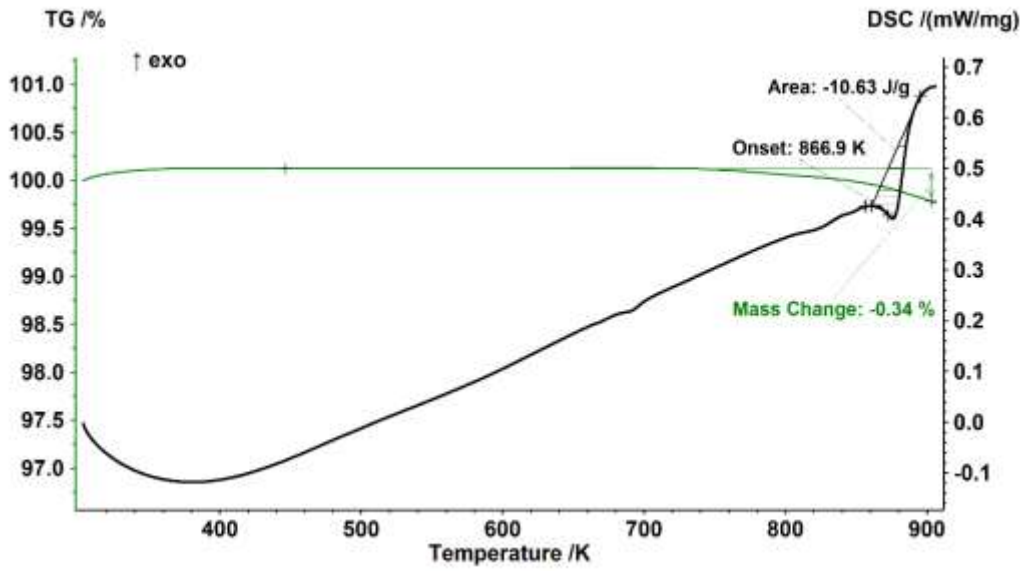

Fig. 4 DSC-TG curve as function of temperature of the Ag_2ZnGeS_4 compound

From the analysis results shown in Figs. 3 and 4 it follows that temperature of phase transition for Ag_2ZnGeS_4 obtained from the DTA measurement (T_{tra} = 869 K) is in agreement with the DSC data (T_{tra} = 866.9 K). A slight difference between the DTA and DSC results for the phase transition of Ag_2ZnGeS_4 is due to the unequal change in the sample composition in the evacuated quartz glass ampule versus under argon pressure in a furnace. Such a difference in the temperature for the phase transition during DTA and DSC measurements was observed earlier for the $Ag_2FeSn_3S_8$ compound [28]. The small deviations on the DSC curve at T ~ 690 K and above 800 K are also correlated with DTA thermal effects. These effects are due to slight equilibrium deviation of the quaternary compound from the stoichiometric composition. From DSC vs T relation, enthalpy of the Ag_2ZnGeS_4 phase transformation has been determined to be $\Delta_{tra}H^o$ = (5.12 ± 0.05) kJ mol^{-1} at T_{tra} = (866.9 ± 1) K. Errors are average accuracies calculated during the temperature and sensitivity calibrations as described in the experimental section. Decimals were rounded to next whole number. As the TG curve in Fig. 4 shows that at pressure of argon P(Ar) = 1·10^5 Pa above T ~ 750 K the Ag_2ZnGeS_4 compound is decomposed due to evaporation of sulfur.

3.2 Thermodynamic Functions

According to the phase equilibria presented in Fig. 1, the virtual reactions in the ECCs (i) and (ii), which contain different compositions of phases from regions (V) and (VI), can be used to calculate the thermodynamic properties of the Ag_2ZnGeS_4. The electrochemical process of the formation of [Ag_2ZnGeS_4 and GeS] from [Ag, GeS_2, and ZnS] in the positive electrode D of the phase region (V) can be written as follows

$2Ag = 2Ag^+ + 2e^-$ left side electrode (reference system)

$2Ag^+ + 2e^- + 2GeS_2 + ZnS = Ag_2ZnGeS_4 + GeS$ right side electrode (sample system)

$2Ag + 2GeS_2 + ZnS = Ag_2ZnGeS_4 + GeS$ overall cell reaction. (1)

The electrochemical process of the formation of [Ag_2ZnGeS_4 and Ge] from [Ag, GeS, and ZnS] in the positive electrode D of the phase region (VI) can be written as follows

$2Ag = 2Ag^+ + 2e^-$ left side electrode (reference system)

$2Ag^+ + 2e^- + 2GeS + ZnS = Ag_2ZnGeS_4 + Ge$ right side electrode (sample system)

$2Ag + 3GeS + ZnS = Ag_2ZnGeS_4 + 2Ge$ overall cell reaction. (2)

The relationship of EMF versus temperature measured with cells (i) and (ii) were approximated by Eqs. 3 and 4, respectively.

E_1/mV = (32.95±2.20) + (437.23±4.39)·10^{-3}T/K $489 \le T \le 514$ (3)

E_2/mV = (78.89±1.94) + (333.1±3.87)·10^{-3}T/K $489 \le T \le 514$ (4)

The Gibbs energies, entropies and enthalpies of the reactions (1) and (2) can be calculated using EMF measurement results [22,23] and the thermodynamic Eqs. (5)-(7):

$$\Delta_r G = -n \cdot F \cdot E \quad (5)$$

$$\Delta_r S = n \cdot F \cdot (dE/dT) \quad (6)$$

$$\Delta_r H = -n \cdot F \cdot [E - (dE/dT)T] \quad (7)$$

where n = 2 is the number of electrons involved in the reactions (1) and (2), F = 96485.33289 C·mol^{-1} is Faraday constant, and E is the EMF of the ECCs.

By assuming $\left(\frac{\partial \Delta_r H}{\partial T}\right)_p = 0$ and $\left(\frac{\partial \Delta_r S}{\partial T}\right)_p = 0$ [23], the thermodynamic function of reactions (1) and (2) were calculated through extrapolation of the linear temperature dependences of the EMF of ECCs to T = 298.15 K and using Eqs. (5)–(7). The results of the calculations are listed in Table 1.

Table 1 Standard thermodynamic values of reactions (1) and (2) at T = 298.15 K and P = 1 atm

Reaction	$-\Delta_r G^\circ$	$-\Delta_r H^\circ$	$\Delta_r S^\circ$
	kJ·mol^{-1}		J·mol^{-1}·K^{-1}
(1)	31.51 ± 0.68	6.36 ± 0.72	84.37 ± 0.85
(2)	34.39 ± 0.60	15.22 ± 0.64	64.28 ± 0.75

Standard Gibbs energy and entropy of reactions (1) and (2) are related to the Gibbs energy of formation and entropy of compounds and pure elements the following equations

$$\Delta_{r(1)}G^\circ = \Delta_f G^\circ_{Ag_2ZnGeS_4} + \Delta_f G^\circ_{GeS} - 2\Delta_f G^\circ_{GeS_2} - \Delta_f G^\circ_{ZnS} \quad (8)$$

$$\Delta_{r(1)}S^\circ = S^\circ_{Ag_2ZnGeS_4} + S^\circ_{GeS} - 2S^\circ_{Ag} - 2S^\circ_{GeS_2} - S^\circ_{ZnS} \quad (9)$$

$$\Delta_{r(2)}G^\circ = \Delta_f G^\circ_{Ag_2ZnGeS_4} - 3\Delta_f G^\circ_{GeS} - \Delta_f G^\circ_{ZnS} \quad (10)$$

$$\Delta_{r(2)}S^\circ = S^\circ_{Ag_2ZnGeS_4} + 2S^\circ_{Ge} - 2S^\circ_{Ag} - 3S^\circ_{GeS} - S^\circ_{ZnS} \quad (11)$$

Eqs. (12)–(15) were obtained from Eqs. (8)–(11).

$$\Delta_f G^\circ_{Ag_2ZnGeS_4} = \Delta_{r(1)}G^\circ - \Delta_f G^\circ_{GeS} + 2\Delta_f G^\circ_{GeS_2} + \Delta_f G^\circ_{ZnS} \quad (12)$$

$$S^\circ_{Ag_2ZnGeS_4} = \Delta_{r(1)}S^\circ - S^\circ_{GeS} + 2S^\circ_{Ag} + 2S^\circ_{GeS_2} + S^\circ_{ZnS} \quad (13)$$

$$\Delta_f G^\circ_{Ag_2ZnGeS_4} = \Delta_{r(2)}G^\circ + 3\Delta_f G^\circ_{GeS} + \Delta_f G^\circ_{ZnS} \quad (14)$$

$$S^\circ_{Ag_2ZnGeS_4} = \Delta_{r(2)}S^\circ - 2S^\circ_{Ge} + 2S^\circ_{Ag} + 3S^\circ_{GeS} + S^\circ_{ZnS} \quad (15)$$

The reaction of formation of the Ag_2ZnGeS_4 compound from pure elements can be written as

$$2Ag + Zn + Ge + 4S = Ag_2ZnGeS_4 \quad (16)$$

Based on reaction (16), the entropy of formation of the Ag_2ZnGeS_4 compound can be calculated as

$$\Delta_f S^\circ_{Ag_2ZnGeS_4} = S^\circ_{Ag_2ZnGeS_4} - 2S^\circ_{Ag} - S^\circ_{Zn} - 3S^\circ_{Ge} - 4S^\circ_{S} \quad (17)$$

By combining Eqs. (5)–(7) and (12)–(15) with Eq. (17), and data of the pure components reported in [29], the standard Gibbs energy of formations of Ag_2ZnGeS_4 compound as a function of temperature in the phase regions (V) and (VI) were calculated, respectively

$$\Delta_f G^\circ_{Ag_2ZnGeS_4}/(\text{kJ·mol}^{-1}) = -(449.2 \pm 2.6) - (50.0 \pm 1.3) \cdot 10^{-3}T/\text{K} \quad (18)$$

$$\Delta_f G^\circ_{Ag_2ZnGeS_4}/(\text{kJ·mol}^{-1}) = -(448.9 \pm 2.4) - (56.8 \pm 0.9) \cdot 10^{-3}T/\text{K} \quad (19)$$

The uncertainties in Eqs. (18) and (19) are standard uncertainties. A comparative summary of the calculated values together with the available literature values is presented in Table 2.

Table 2 Standard thermodynamic properties of the selected phases in the Ag–Zn–Ge–S system at T = 298.15 K

Phase	$-\Delta_f G^\circ$	$-\Delta_f H^\circ$	S°	[Ref]
	kJ mol^{-1}		J mol^{-1} K^{-1}	Note
Ag	0	0	42.677	[29]
Zn	0	0	41.631	[29]
Ge	0	0	31.087	[29]
S	0	0	32.056	[29]
GeS	76.995	76.149	65.982	[29]
GeS_2	154.588	156.900	87.446	[29]
ZnS	200.403	205.183	57.656	[29]
Ag_2ZnGeS_4*	464.1 ± 2.5	449.2 ± 2.6	336.3 ± 1.3	This work
Ag_2ZnGeS_4**	465.8 ± 2.3	448.9 ± 2.4	343.1 ± 0.9	This work

* phase region (V)
** phase region (VI)

The calculated values of the Gibbs energy and enthalpy of the Ag_2ZnGeS_4 compound in both phase regions are consistent. The difference in the entropies is somewhat higher and does not exceed ~2%. Based on these results it was concluded that Ag_2ZnGeS_4 has stoichiometric composition.

Conclusions

Phase equilibria in the ZnS–Ag_2GeS_3–Ge–GeS_2 part of the Ag–Zn–Ge–S system were established by applying DTA, XRD, and EMF methods. The phase diagram along the Ag_2GeS_3–ZnS cross-section was constructed and thermal stability of the Ag_2ZnGeS_4 compound was established. The measured EMF versus temperature values were used to calculate the Gibbs energies of formation of the Ag_2ZnGeS_4 compound in the Ag_2ZnGeS_4–GeS–GeS_2–ZnS and Ag_2ZnGeS_4–GeS–Ge–ZnS phase regions. The thermodynamic functions of the quaternary compound in both phase regions are consistent. This consistency indicates that Ag_2ZnGeS_4 has stoichiometric composition. The experimental thermodynamic functions of the quaternary phase determined in this work supplement data for complete thermodynamic modeling of the *T*–*x* phase diagrams of the Ag–Zn–Ge–S system.

Acknowledgements

The authors are grateful to the Academy of Finland for financial support. This work was made under the project "Thermodynamic investigation of complex inorganic material systems for improved renewable energy and metals production processes" (Decision number 311537) as part of the activities of the Johan Gadolin Process Chemistry Centre at Åbo Akademi University. In addition, funding from the Academy of Finland project "Behavior and properties of molten ash in biomass and waste combustion" (Decision number 266384) for M. Moroz and D. Lindberg is greatly appreciated.

Conflict of Interest

The authors declare that they have no conflict of interest.

References

1. I. Tsuji, Y. Shimodaira, H. Kato, H. Kobayashi, and A. Kudo, Chem. Mater. **22**, 1402 (2010).
2. O. V. Parasyuk, A. O. Fedorchuk, Y. M. Kogut, L. V. Piskach, and I. D. Olekseyuk, J. Alloys Compd. **500**, 26 (2010).
3. M. Himmrich and H. Haeuseler, Spectrochim. Acta Part Mol. Spectrosc. **47**, 933 (1991).
4. S. Chen, X. G. Gong, A. Walsh, and S.-H. Wei, Phys. Rev. B **79**, (2009).
5. Q. Guo, H. W. Hillhouse, and R. Agrawal, J. Am. Chem. Soc. **131**, 11672 (2009).
6. X. Fontané, V. Izquierdo-Roca, E. Saucedo, S. Schorr, V. O. Yukhymchuk, M. Y. Valakh, A. Pérez-Rodríguez, and J. R. Morante, J. Alloys Compd. **539**, 190 (2012).
7. F.-J. Fan, L. Wu, and S.-H. Yu, Energy Env. Sci **7**, 190 (2014).
8. K. Zhang and L. Guo, Catal. Sci. Technol. **3**, 1672 (2013).
9. G. E. Davydyuk, G. L. Myronchuk, I. V. Kityk, S. P. Danyl'chuk, V. V. Bozhko, and O. V. Parasyuk, Opt. Mater. **33**, 1302 (2011).

10. O. V. Parasyuk, L. V. Piskach, I. D. Olekseyuk, and V. I. Pekhnyo, J. Alloys Compd. **397**, 95 (2005).
11. O. V. Parasyuk, L. D. Gulay, L. V. Piskach, and O. P. Gagalovska, J. Alloys Compd. **336**, 213 (2002).
12. L. V. Piskach, O. V. Parasyuk, I. D. Olekseyuk, Y. E. Romanyuk, S. V. Volkov, and V. I. Pekhnyo, J. Alloys Compd. **421**, 98 (2006).
13. H. Ipser, A. Mikula, and I. Katayama, Calphad **34**, 271 (2010).
14. A. Kroupa, Comput. Mater. Sci. **66**, 3 (2013).
15. E. Robinel, B. Carette, and M. Ribes, J. Non-Cryst. Solids **57**, 49 (1983).
16. M. Moroz, F. Tesfaye, P. Demchenko, M. Prokhorenko, D. Lindberg, O. Reshetnyak, and L. Hupa, J. Chem. Thermodyn. **118**, 255 (2018).
17. A. G. Mikolaichuk, N. V. Moroz, P. Y. Demchenko, L. G. Akselrud, and R. E. Gladyshevskii, Inorg. Mater. **46**, 590 (2010).
18. H. Preston-Thomas, Metrologia **27**, 3 (1990).
19. Diffractom. Stoe WinXPOW Version 303 Stoe Cie GmbH Darmstadt 2010 (n.d.).
20. W. Kraus and G. Nolze, POWDER CELL – Program Represent. Manip. Cryst. Struct. Calc. Resulting X-Ray Powder Patterns **29**, 301 (1996).
21. P. Villars and K. Cenzual, editors , *Pearson's Crystal Data: Crystal Structure Database for Inorganic Compounds, Release 2014/15*, ASM International, Materials Park (Ohio, USA, 2014).
22. M. B. Babanly, Y. A. Yusibov, and N. B. Babanly, in *Electromotive Force Meas. Several Syst.*, edited by S. Kara, InTech (2011), pp. 57–78.
23. E. G. Osadchii and E. A. Echmaeva, Am. Mineral. **92**, 640 (2007).
24. M. V. Moroz, M. V. Prokhorenko, and S. V. Prokhorenko, Russ. J. Electrochem. **51**, 886 (2015).
25. M. V. Moroz, M. V. Prokhorenko, O. V. Reshetnyak, and P. Y. Demchenko, J. Solid State Electrochem. **21**, 833 (2017).
26. M. B. Babanly, L. F. Mashadieva, Z. S. Aliev, A. V. Shevelkov, and Y. A. Yusibov, J. Alloys Compd. **524**, 38 (2012).
27. F. Tesfaye and P. Taskinen, J. Solid State Electrochem. **18**, 1683 (2014).
28. M. Moroz, F. Tesfaye, P. Demchenko, M. Prokhorenko, D. Lindberg, O. Reshetnyak, and L. Hupa, J. Electron. Mater. **47**, 5433 (2018).
29. I. Barin, *Thermochemical Data of Pure Substance*, VCH, Weinheim (1995).